

Research Paper

Photobiomodulation Therapy Restores Olfactory Function Impaired by Photothrombosis in Mouse Olfactory Bulb

Reham A. Shalaby^a, Muhammad Mohsin Qureshi^b, Mohd. Afzal Khan^a, S.M. Abdus Salam^c, Hyuk Sang Kwon^a, Kyung Hwa Lee^{c,**}, Euiheon Chung^{a,d,*}, Young Ro Kim^e

^a Department of Biomedical Science and Engineering, Gwangju Institute of Science and Technology, South Korea

^b Division of Biophysics and Bioimaging, Princess Margaret Cancer Center, Toronto, Ontario, Canada

^c Department of Pathology, Chonnam National University, Hwasun Hospital and Medical School, BioMedical Sciences Graduate Program (BMSGP), South Korea

^d AI Graduate School, Gwangju Institute of Science and Technology, South Korea

^e Department of Radiology, Harvard Medical School, Boston, MA, USA



ARTICLE INFO

Keywords:

Ischemic stroke
Olfactory dysfunction
Photothrombosis
Photobiomodulation
Buried food test
Olfactory bulb
Neuroinflammation

ABSTRACT

An ischemic stroke typically accompanies numerous disorders ranging from somatosensory dysfunction to cognitive impairments, inflicting patients with various neurologic symptoms. Among pathologic outcomes, post-stroke olfactory dysfunctions are frequently observed. Despite the well-known prevalence, therapy options for such compromised olfaction are limited, likely due to the complexity of olfactory bulb architecture, which encompasses both the peripheral and central nervous systems. As photobiomodulation (PBM) emerged for treating ischemia-associated symptoms, the effectiveness of PBM on stroke-induced impairment of olfactory function was explored. Novel mouse models with olfactory dysfunctions were prepared using photothrombosis (PT) in the olfactory bulb on day 0. The post-PT PBM was performed daily from day 2 to day 7 by irradiating the olfactory bulb via an 808 nm laser with a fluence of 40 J/cm² (325 mW/cm² for 2 s/min per day). The buried food test (BFT) was used to score behavioral acuity in food-deprived mice to assess the olfactory function before PT, after PT, and after PBM. Histopathological examinations and cytokine assays were performed on the mouse brains harvested on day 8. The results from BFT were specific to an individual, with positive correlations between the baseline latency time measured before PT and its alteration at the ensuing stages for both the PT and PT + PBM groups. Also, the correlation analysis in both groups showed highly similar, significant positive relationships between the early and late latency time change independent of PBM, implicating a common recovery mechanism. Particularly, PBM treatment accelerated the recovery of impaired olfaction following PT by suppressing inflammatory cytokines and enhancing both glial and vascular factors (e.g., GFAP, IBA-1, and CD31). PBM therapy during the acute phase of ischemia improves the compromised olfactory function by modulating microenvironments and inflammation status of the affected tissue.

1. Introduction

Photobiomodulation (PBM) is a drug-free light therapy that is well-documented for its beneficial effects via endogenous self-repair mechanisms (Eissa and Salih, 2017). Numerous studies have demonstrated the therapeutic efficacy of PBM, which spans across a wide range of measures in both structural and functional recoveries. The PBM therapy-associated biological alterations include the reduction of inflammation and oxidative stress, as well as the improvement of mitochondrial

function (Ferraesi et al., 2015; Thunshelle and Hamblin, 2016; Hamblin, 2017). Moreover, previous clinical reports also indicated treatment benefits by multiple exposures, such as the stimulation of wound healing (Hopkins et al., 2004), pain alleviation in various orthopedic and musculoskeletal conditions (Aimbire et al., 2006), and restoration of brain function (Lapchak, 2010).

From the neurological aspect, the efficacy of PBM has been shown in treating the traumatic brain injury with outcomes including increases in the cerebral volume and perfusion, and improvements in the functional

* Corresponding author at: 123 Cheomdan-gwagiro, Buk-gu, Gwangju 61005, South Korea.

** Corresponding author at: 322, Seoyang-ro, Hwasun-eup, Hwasun-gun, Jeollanam-do 58128, South Korea.

E-mail addresses: mdkaylee@jnu.ac.kr (K.H. Lee), ogong50@gist.ac.kr (E. Chung).

connectivity and cognitive faculties (Naeser et al., 2011; Chao et al., 2020). PBM is also known to be effective in the management of patients with Alzheimer's dementia by boosting executive function, memory, visual attention, and connectivity measures (Berman et al., 2017; Hamblin, 2019). Additionally, preclinical studies revealed that the PBM therapy could be also effective in Parkinson's disease (Salehpour and Hamblin, 2020) and ischemic stroke (Yang and Crawley, 2009; Kim et al., 2022). In particular, previous stroke model studies revealed that the PBM therapy reduces behavioral deficits while promoting neurogenesis (Yang et al., 2018). Although emerging as one of promising candidates for treating stroke-associated functional impairments, mechanisms of action underlying such recovery have been elusive.

In this regard, using a novel animal stroke model with function-specific damage, our current study aims to address the utility of PBM by demonstrating the direct behavioral/functional recovery in conjunction with histopathological assays. We targeted the olfactory bulb (OB) as our stroke site of interest. However, OB possesses a complex structure with multiple layers of interconnecting cell types such as olfactory nerve layer, glomerular layer, mitral cell layer, and granule cell layer. The neuron's turnover rate in the mouse OB is primarily driven by neural stem cells that differentiate into mature interneurons, and other transmission and output neurons, including mitral and tufted cells. (Brann and Firestein, 2014). Olfactory epithelial cells, such as supporting cells, basal cells and olfactory receptor neurons (ORNs) are continually replaced throughout lifetime. In rodents, the turnover rate for olfactory epithelium and ORNs has been estimated to be around 30–60 days (Graziadei and Graziadei, 1979; Brann and Firestein, 2014). However, the turnover of OB neurons in adult mice is not well-characterized. While the turnover rate can be influenced by various factors such as exposure to novel odors or injury to the olfactory epithelium, astrocytes have also been shown to play a role in the regeneration.

The profound prevalence of post-stroke olfactory dysfunction is present in 43.6% of the stroke patients, a year after the insult (Wehling et al., 2015). Chien-FU Yeh et al. also reported that olfactory dysfunction after MCAO stroke model was explained by the low mRNA expression of olfactory marker protein and the high mRNA expression of microglia/macrophage activation and proinflammatory mediators (Yeh et al., 2019). Additionally, such olfactory dysfunction is also commonly observed in patients with Alzheimer's disease (Wesson et al., 2010), Parkinson's disease (Doty, 2012), and frontotemporal dementia (Carnemolla et al., 2020). Reports also suggested that the impaired olfaction is linked with cognitive decline and might be used as an indicator of neurodegeneration among dementia-free older adults (Dintica et al., 2019). More recently, pre-symptomatic and aftereffect olfactory dysfunctions in Covid-19 patients have been recognized as common traits of the disease, further augmenting the need for developing effective therapeutic strategies to treat the olfaction related impairments (Rebholz et al., 2020).

To induce an olfactory function loss via highly controlled formation of the ischemic stroke, we adopted photothrombosis (PT) precisely at the OB to which the localized PBM therapy was directly applied daily. Following the PT induction, behavioral measurements, immunohistochemistry, and cytokine assays were performed to explore the factors involved with functional changes. The importance of our current work lies in the experimental demonstration to answer whether the PBM therapy influences the recovery of impaired olfactory function while affecting the associated biological/biochemical factors. Positive outcome of the proposed non-invasive PBM approach would strongly benefit patients suffering from olfactory symptoms derived from stroke and other neurodegenerative diseases.

2. Methods

All experimental protocols followed the guidelines of the Institutional Animal Care and Use Committee (IACUC) at Gwangju Institute of

Science and Technology (GIST), Korea. The experimental protocols were approved by the GIST IACUC under protocol # GIST-2020-077. We used 73 C57BL/6 male mice aged between 10 and 12 weeks. Seven mice were excluded because 3 mice became inactive after fasting 18 h at D3, 2 mice died at D1 after PT and 2 mice died at the first time of PBM. All mice were 25–30 g in body weight.

2.1. Buried food test (BFT) for olfactory function measurement

The buried food test (BFT) was performed according to the previously published protocol (Yang and Crawley, 2009). Adaptation to food was achieved by introducing the food pellets with fresh odor daily to the mice for one week. On the test day, animals were fasted (except for water) for 18 h and then introduced to a clean mouse cage where an odorous food pellet (RodFeed, DBL, Chungcheongbuk-do, South Korea) was randomly embedded under the 3 cm thickness of clean bedding. Then, latency in the food search time was measured, which was repeated three times for each BFT session. The first BFT after PT was performed three days after the PT since certain mice were inactive after their PT surgeries. So the time was taken to allow the mice to recover, as shown in Fig. 1A and B. We measured the body weight before each BFT to assess the weight fluctuation after 18 h of fasting. The BFT was conducted on day – 1 before the PT induction to obtain the baseline which was followed by the BFTs on day 3 and 7 post-PT.

2.2. Olfactory bulb (OB) photothrombosis

Photothrombosis (PT) was performed on day 0 for both PT and PT + PBM groups. An incision was made in the scalp over the OB area between two eyelids; the periosteum was gently removed using a scalpel. Then a 4 mm coverslip was fixed over the OB area and sealed with glue. A retro-orbital injection of 20 mg/kg of rose Bengal was given to the PT group, after which a green 532 nm laser was illuminated over the coverslip for 15 min in a dark room, as shown in Fig. 1C. Then, each mouse was transferred to a new cage and placed for recovery. The identical protocol was used for the control group, except for the rose Bengal injection. The body temperature was maintained at $37 \pm 0.5^\circ\text{C}$ throughout the procedures.

2.3. Photobiomodulation after photothrombosis in olfactory bulb

Photobiomodulation was performed daily using an 808 nm laser from day 2 to 7 post-PT for 2 min per day. The fluence was 40 J/cm^2 per session, where the laser beam diameter was $4.17 \pm 0.07\text{ mm}$ with the irradiance of 325 mW/cm^2 , as shown in Fig. 1D. The PBM was performed in a dark room while maintaining the body temperature at $37 \pm 0.5^\circ\text{C}$. A holed black mask was used over the OB area to protect the surrounding tissue from unnecessary light exposures.

2.4. Photobiomodulation in sham control mice

The PBM control group was prepared with the same surgery and by placing the coverslip over the OB but without inducing the photothrombotic ischemia (i.e., excluding the illumination of a 532 nm laser and injection of rose bengal). Using an 808 nm laser, PBM was similarly applied in this control group from day 2 to 7 (i.e., Sham Control +PBM), while performing the BFT to evaluate functional changes.

2.5. Brain sampling

On day 8, mouse brains were harvested after the heart perfusion with 4% paraformaldehyde solution (PFA) and fixed in 10% neutral-buffered formalin for three days. Then, the brains were dissected, embedded in paraffin, and stained with hematoxylin and eosin (H&E) for histologic examination. For the cytokine assay, brains were extracted on day 8 without the perfusion and immediately kept in a -80°C freezer.

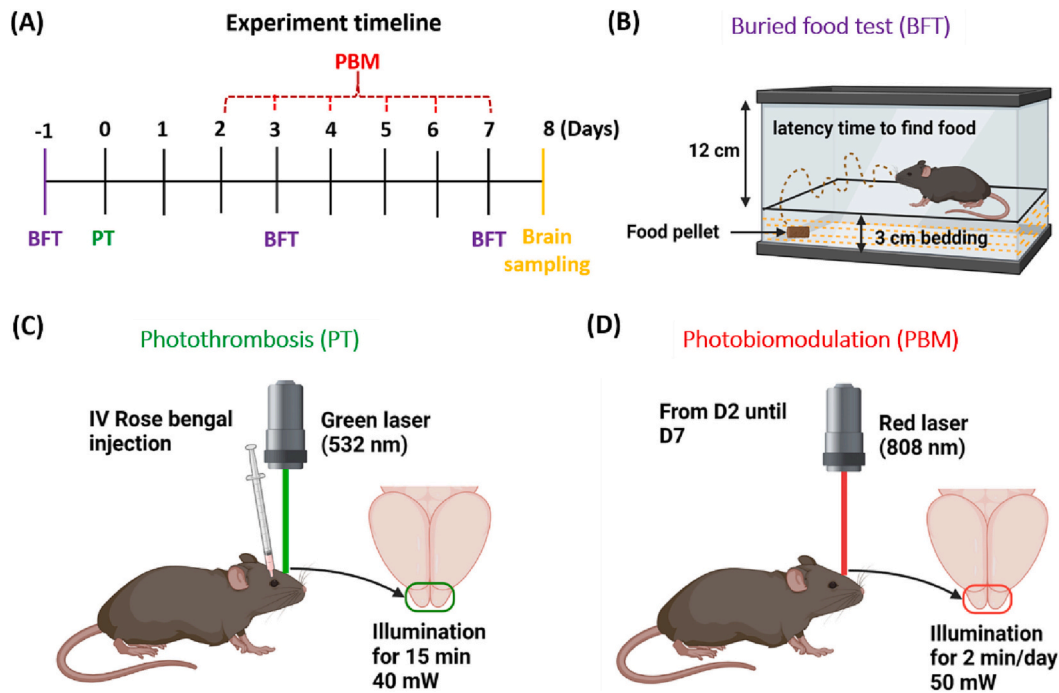


Fig. 1. Schematic diagram of experimental design. (A) Experimental timeline of olfactory function test (i.e., buried food test: BFT), photothrombosis (PT), photobiomodulation (PBM), and brain sampling. (B) Illustration of BFT. (C) Photothrombosis parameters using a 532 nm green laser. (D) Photobiomodulation parameters using an 808 nm red laser. (For interpretation of the references to colour in this figure legend, the reader is referred to the web version of this article.)

2.6. Cytokine assay

The post-PT cytokine levels were assessed on day 8 using the OB tissue lysates obtained from the control, PT, and PT + PBM groups. The cytokine expressions were analyzed by Proteome Profiler Mouse Cytokine Array Panel A Kit (ARY006, R&D Systems) on 9 samples (3 from each group). The assay was performed following the manufacturer's instructions to pool the samples together and each cytokine is represented by 2 consecutive expression values. Expression levels were analyzed densitometrically using Image J, after being corrected by the values determined in positive controls and expressed as relative values compared to the control group.

2.7. Immunohistochemistry

Paraffin blocks of mouse brains were cut in 3 μ m thickness and subjected to immunohistochemistry (IHC). Tissue sections were stained with antibodies against Glial Fibrillary Acidic Protein (GFAP) (dilution 1:400, code no. M0761, Dako, Glostrup, Denmark), IBA1 (dilution 1:400, code no. 234-003, Synaptic Systems, Goettingen, Germany) and CD31 (dilution 1:200, code no. M0823, Dako) using the Bond-max system (Leica Microsystems, Bannockburn, IL, USA). Negative controls were processed similarly in the absence of primary antibodies. The resulting slides were evaluated by a clinical pathologist (KHL), which were digitalized using a slide scanner (Aperio ScanScope CS System, Leica Microsystems) and photographed by the Aperio Image Scope 12.3 (Leica). For the analysis of IHC, three ROI's in the stained image were selected to reflect the heterogeneous distribution for each OB at \sim 200 μ m from the lesion, corresponding to the area surrounding the lesion (i.e., peri-infarct area). To analyze images of GFAP and IBA-1, Image J (Fiji) software was used for the quantitative evaluation of immunoreactivity. The images were inverted using Image J, and the numbers of immune-positive cells were counted with a multi-point tool. For the CD31 quantification, automated analyses were performed to count the number and mean area of the vessels using a homemade algorithm and the open CV library.

2.8. Statistical analysis

Statistical analysis for determining group differences was performed using one-way analysis of variance (ANOVA) tool in the GraphPad Prism software unless otherwise specified. Student's *t*-tests were used when two groups were compared for the difference, all comparisons were tested for normality and variance homogeneity using the same Graphpad Prism software. Statistical significance was accepted at the 95% confidence level ($P < 0.05$). Data were expressed as means \pm SD.

3. Results

3.1. Development of olfactory bulb photothrombosis model

We developed a novel rodent model of OB ischemia based on PT using a 532 nm green laser, as shown in Fig. 2. Since the green laser beam profile is directly linked with the formation of ischemic damage, the spatial laser beam profile was characterized and tested for repeatability. The diameter of the 532 nm laser beam used in our study was 3.9 ± 0.1 mm. In order to quantify the olfactory function and to explore the ideal time of intervention with PBM and also the proper time for brain sampling, we utilized the BFT and measured the latency times on the day before PT (D-1), day 3 (D3), D7, and D14 after PT. As shown in Fig. 2C, the latency time (i.e., the time taken before the discovery of hidden food) significantly increased on D3 compared to the control value before PT (i.e., D-1) for the PT group, which was slightly but significantly reduced on D7 when compared to D3. Between the D7 and D14, no further change in the latency time was observed. The H & E staining provided the detailed description of the tissue alterations after PT, revealing an abnormal tissue morphology with degenerative features, in contrast to those found in the normal controls as shown in Fig. 2D.

3.2. PBM significantly improves behavioral deficits after PT

As shown in Fig. 3, in normal control (NC) mice, the latency time did

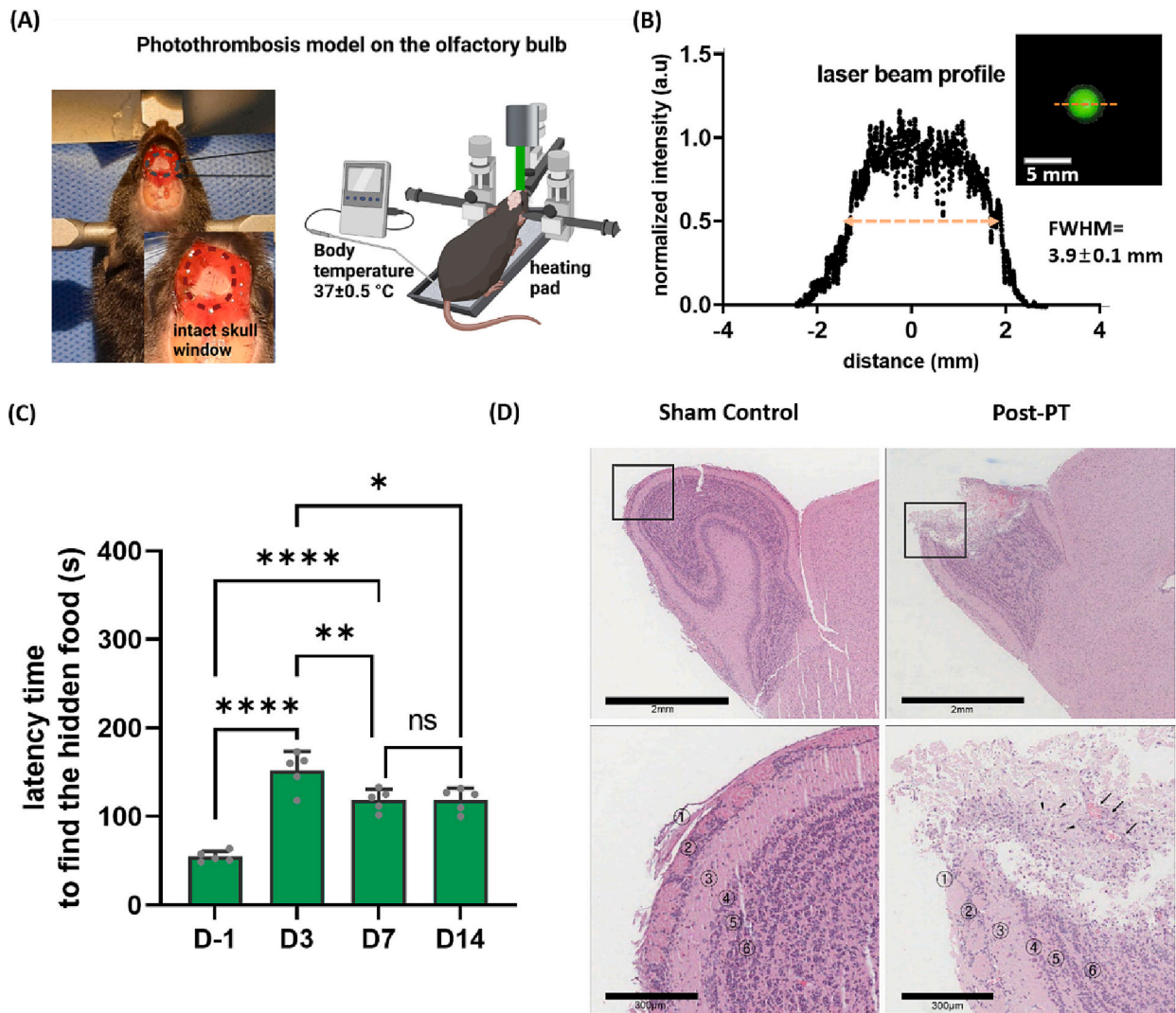


Fig. 2. Olfactory bulb photothrombosis model. (A) Photothrombosis setup and parameters. (B) 532nm laser beam profile during OB illumination. (C) Olfactory function test results after photothrombosis, $n = 5$. (D) H&E staining of OB sections of normal control OB and post-PT OB obtained on Day 8. The rectangular area in each panel is magnified in the corresponding high-magnification photograph below. High-magnification photographs of OB sections (lower panels) indicate the six layers that make up the mouse olfactory bulb are shown: ① olfactory nerve layer, ② glomerular layer, ③ external plexiform layer, ④ mitral cell layer, ⑤ internal plexiform layer, ⑥ granule cell layer. In the post-PT mouse OB, vascular proliferation (arrows) and foamy macrophage infiltration (arrowheads) are observed, along with necrotic changes in the damaged tissue. Notably, all six layers seen in normal tissue are destroyed. Data are mean \pm SD. ($n = 5$; $*P < 0.05$, $**P < 0.01$, $***P < 0.0001$; ns-not significant)

not vary throughout the test days, confirming the reference stability of BFT over time. For the sham control (SC) group, the olfactory function was unaffected after the 532 nm laser exposure as also, no PBM-related alterations were found in the normal, healthy olfactory function of the SC + PBM mice. The findings reveal that the laser exposures caused little influence on the normal olfaction, in which PBM using an 808 nm laser was applied between D2 and D7 after surgery for 2 min per day.

The BFT's were performed on D - 1, D3, and D7 to investigate the impact of PBM following PT. The latency time measured on D3 for the PT mice significantly increased compared to that of the baseline (D-1). In comparison with the PT group, the PT + PBM group exhibited a significant improvement in the olfactory function on D3. For the PT mice, the significantly deteriorated olfactory function on D3 only improved with a slight and non-significant latency time change between D3 to D7 as in Fig. 3A. Of a note, the latency time on D7 was significantly longer than that of the baseline (D-1) in the PT group whereas these values were similar for PT + PBM. Upon comparison with the PT group, significantly greater improvements of the impaired olfactory function were observed on both D3 and D7 in the PT + PBM group. In particular,

the significantly improved olfactory function on D3 revealed a clear, positive effect even by a single, one-time PBM treatment (see the comparison between PT and PT + PBM groups in Fig. 3A).

As shown in Fig. 3B, the relative latency time was measured to eliminate the inter-animal variations by normalizing the latency time after surgery with the baseline latency time to find there is no significance between D3 and D7 in PT group, while there is a significant improvement at D7 in the olfactory function in PT + PBM group. In Fig. 3C, a quantitative analysis revealed that the latency time changes from the baselines were significantly different between the PT and PT + PBM groups only on D7 (after six sessions of PBM). Such group differences of the latency time changes were not pronounced in other periods (i.e., $t_{D3-t_{D-1}}$ and $t_{D3-t_{D7}}$), implicating the efficacy of the long term PBM therapy. In addition, it was notable that for both PT and PT + PBM groups, the outcomes of BFT were specific and able to delineate the individual differences, as the significant positive correlation was found between the baseline and changes in the latency time (see Fig. 3B and supplementary Fig. S3).

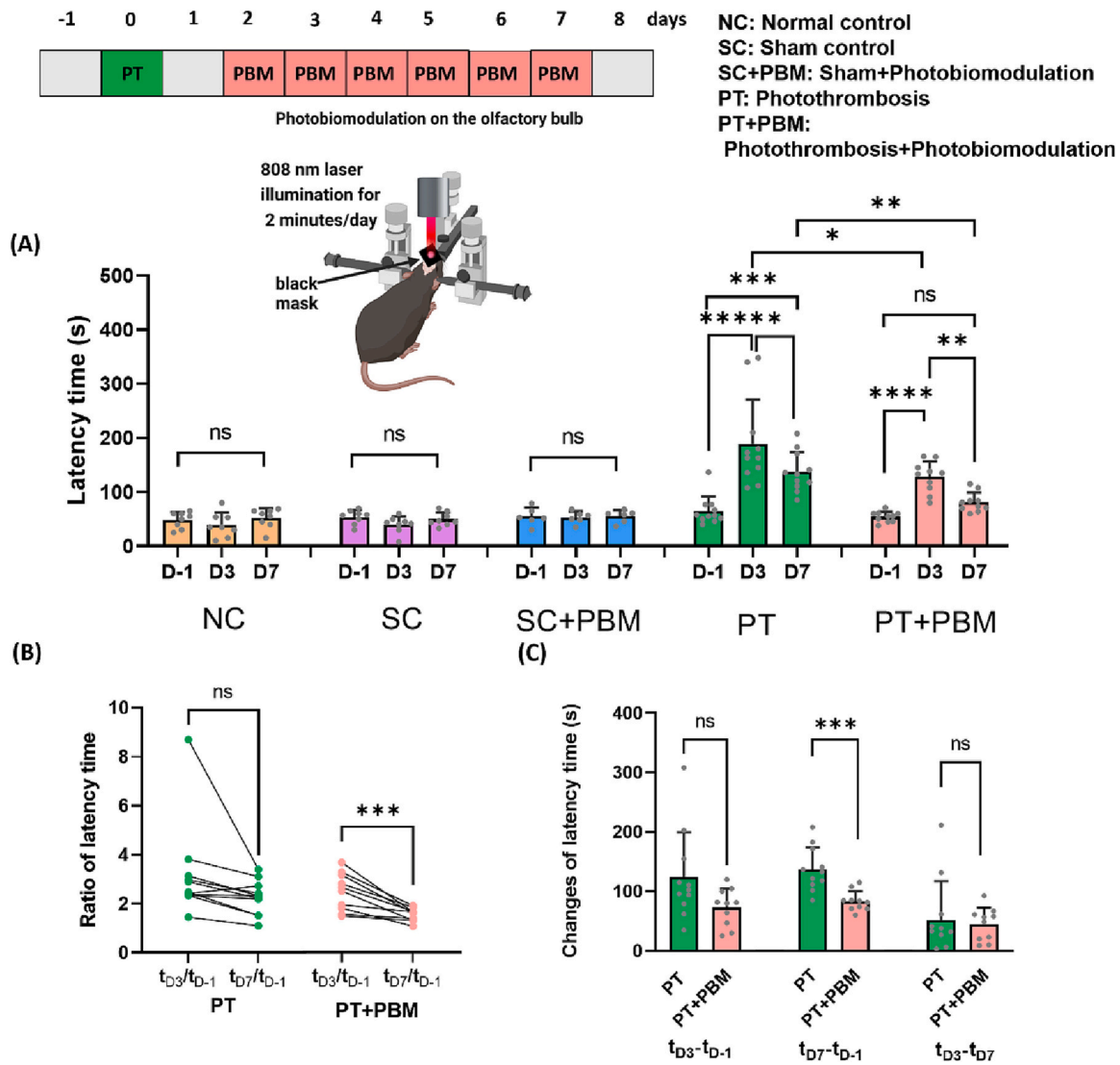


Fig. 3. Effects of PBM on behavioral deficits after PT. (A) Buried food test results for all experimental groups over time, NC: $n = 8$, SC: $n = 8$, SC + PBM: $n = 6$, PT: $n = 11$, PT + PBM: $n = 10$. (B) Analysis of the ratio of latency time based on the baseline function for PT and PT + PBM groups. (C) Olfactory function test results from the changes of the latency times for the PT and PT + PBM groups. Data are mean \pm SD. (* $P < 0.05$, *** $P < 0.001$, **** $P < 0.0001$; ns-not significant, (A) Two-way ANOVA test, (B) paired t -test, (C) student's t -test)

3.3. Correlation analysis of the latency time changes

Correlation analyses among the latency time changes revealed that there were significant, a positively correlative relationship in the changes of the latency time between the early (D-1 and D3) and late (D3 and D7)

and D7) periods as shown in Fig. 4 (A) and (B). The PT + PBM figure shows a leftward shift compared to the PT figure, indicating that PBM potentially mitigated early phase impairment of the olfactory function, even after a single exposure to PBM. No other significant relationships were found upon analyzing the correlation among the latency times and

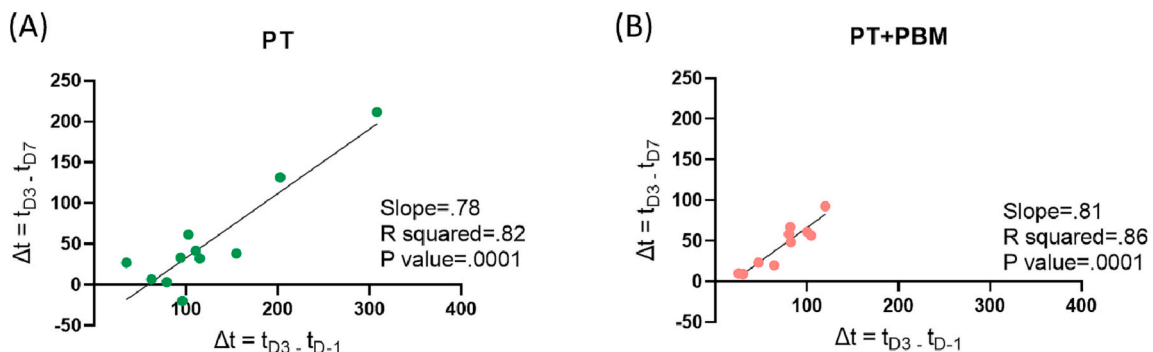


Fig. 4. Correlation of changes in the latency time between the early (D-1 and D3) and late (D3 and D7) periods for (A) PT and (B) PT + PBM groups.

baselines.

3.4. PBM has anti-inflammatory effects after PT

As shown in Fig. 5, higher expression levels of inflammatory cytokines (e.g., C5/C5a, IL-1 α , IL-1 β , IL-16, etc.) were detected in the PT group when compared to the control group. As demonstrated by the PT + PBM group, such inflammatory cytokine levels tended to decrease by PBM. For certain cytokines (e.g., IL-16, IL-17, IFN- γ , TNF- α), the expression levels were restored by PBM near to the control levels. The anti-inflammatory mediators were not altered by PT but responded to PBM, in which cytokines including GM-CSF, IL-1ra, IL-4 and IL-10 were up-regulated to the levels higher than those from the control group (Figs. 5C). In addition, we also found that sICAM-1, the soluble form of cellular adhesion molecule, a useful marker of endothelial activation and inflammation was highly expressed after PBM (Figs. 5A). Thus, PBM did not only inhibit the post-PT inflammatory activities but also promoted anti-inflammatory effects.

3.5. PBM enhances microenvironment recovery after PT

As shown in Fig. 6A–D, glial fibrillary acidic protein (GFAP: present mostly in reactive astrocytes) expression was significantly higher in the PT group than either the control or the PT + PBM group measurements,

implicating the suppression of the post-PT astrocyte activation by PBM. In Fig. 6E–H, the expression of allograft inflammatory factor 1 (IBA-1), responsible for injury repair was significantly higher in both PT and PT + PBM groups than control. Such trend suggested the highly enhanced post-PT activation of microglia, which was unhampered by the PBM treatment. As shown in Fig. 7A–C, our results additionally demonstrated that the stains of CD31 expression in the PT + PBM group was more densely populated than that found in the PT group. And both the microvascular density and demarcated area were significantly higher in the PT + PBM group than PT, exhibiting post-PT restoration of the microvascular matrix by PBM.

4. Discussion

The current study was designed to explore the therapeutic efficacy of photomodulation for treating olfactory dysfunctions. One of the primary aims in our study was to investigate the effects of PBM on neurofunctional impairments using an animal model that mimics human brain disease conditions. In this regard, we developed a new animal model by precluding the use of any unnatural intervention, such as genetic engineering or chemical modifications, which are common in Parkinson's and Alzheimer's disease (LaFerla and Green, 2012; Blesa and Przedborski, 2014). For this purpose, we chose to utilize focal ischemia, which selectively disrupts the neural function via occlusion of the local blood

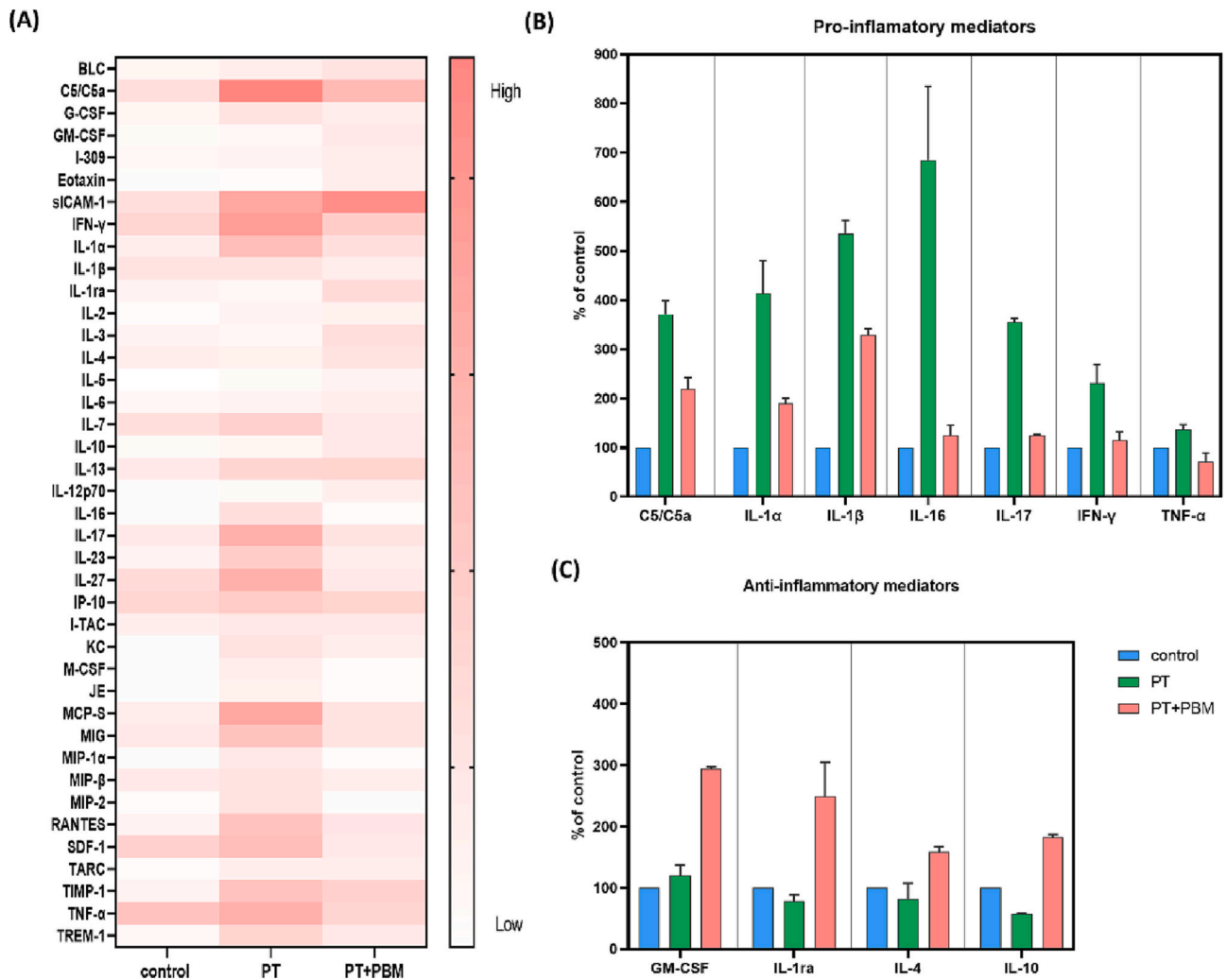


Fig. 5. The effect of PBM on cytokines after PT. (A) Heat map visualization of cytokines and chemokines for control, PT and PT + PM mice. (B) The normalized cytokine expression with respect to the control group (%) of PT and PBM on the pro-inflammatory and (C) anti-inflammatory mediators. Samples were collected on day 8. Data are expressed as mean \pm SD. *n* = 3/group.

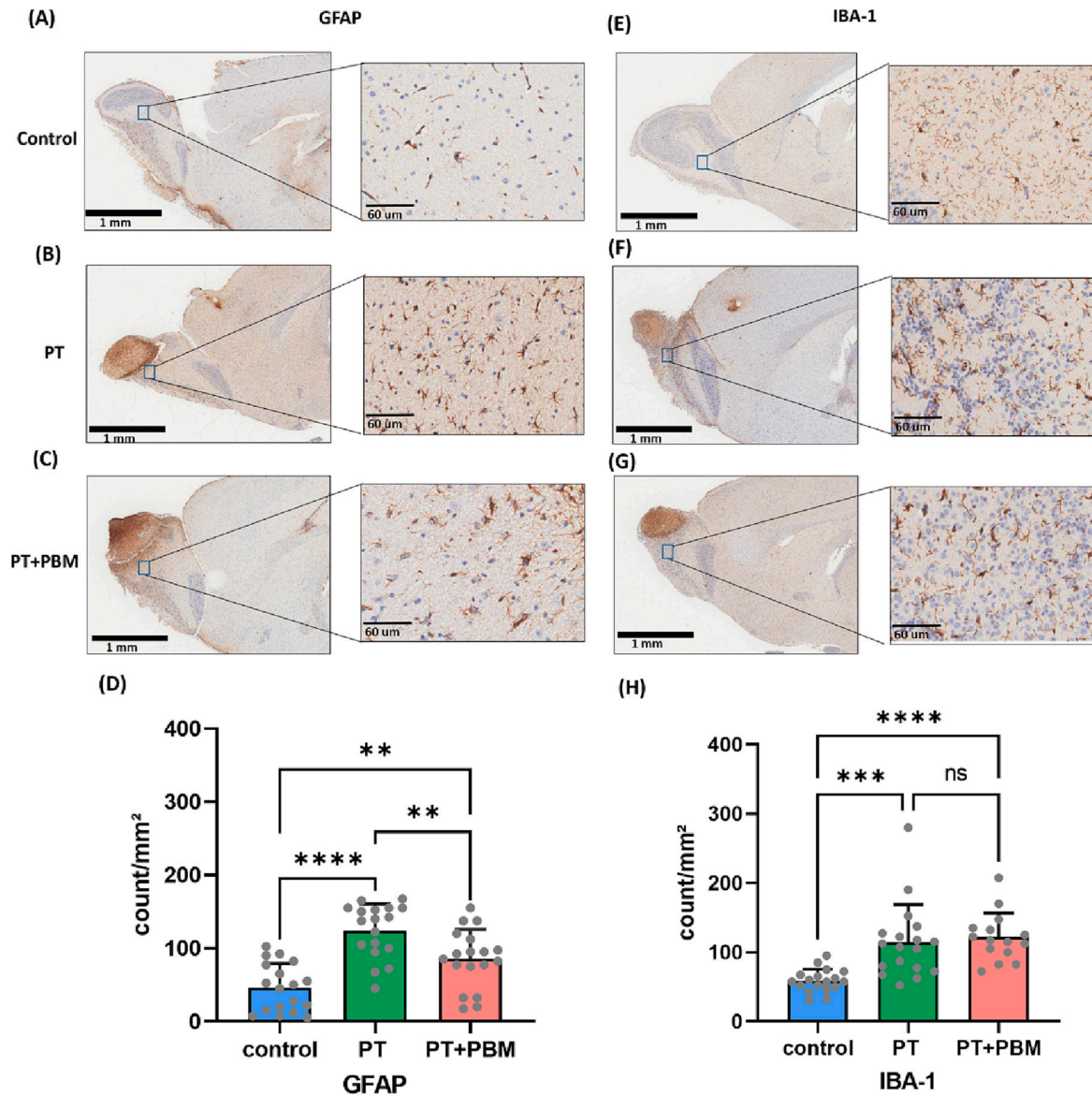


Fig. 6. PBM manipulates the activation of non-neuronal cells after PT. (A-C) Expression of GFAP in control, PT, PT + PBM with high magnification images. (D) Quantitative analysis of GFAP. (E-G) Expression of IBA-1 in control, PT, PT + PBM. (H) Quantitative analysis of IBA-1. Samples were collected on day 8. Data are expressed as mean \pm SD. ($n = 6$ animal per group, 3 areas per animal; * $P < 0.05$, ** $P < 0.01$, *** $P < 0.001$, **** $P < 0.0001$; ns-not significant).

flow.

In particular, to increase the specificity of the functional deficit, we induced photothrombosis (PT), which was regionally confined in the olfactory bulb of mouse. Highly precise for damaging the brain area of interest, it is also notable that the PT-induced stroke produces a relatively small ischemic penumbra (Labat-gest and Tomasi, 2013). Since penumbral peri-infarct areas are known to be involved in the recovery process, the lack of such might have limited the current study in the inexact pathological reproduction of human stroke conditions. However, compared with other traditional stroke methods, such as filament occlusion, the PT-induced lesions were highly reproducible for maintaining the consistent infarct size and location, only impairing the olfactory function as proposed in our study. Such specificity of PT was highly important to confine the study focus concentrated on the examination of factors that are strictly associated with the olfaction behavior.

As for assessing the functional deficit, buried food test (BFT) has been used frequently to quantify behavioral acuity of the olfactory function (Alberts and Galef Jr., 1971). While there is a controversy due to the possible reliance on locational memory, in the current study, such

shortcoming was mitigated by randomly placing the food pellet and also by measuring the latency time three times at each trial. A few previous studies have indicated that even a single dose of photonic therapy could confer beneficial effects on brain injuries, independent of the therapy time point after the disease onset. Similarly, in the current PT model, functional improvements were induced by a single PBM treatment on post-PT D3 (see Fig. 3A), in agreement with reports from previous studies (Lapchak et al., 2007; Oron et al., 2012; Xuan et al., 2015; Hamblin, 2016). Moreover, by tracking down the changes in individual performance over the course of post-PT measurements (e.g., excluding the baseline contribution), we were able to delineate subtle functional alterations. Upon comparing the PT group with PT + PBM based on such approaches, effects of the PBM treatments were demonstrated with a particular functional improvement on D7, which was not observed on D3 as shown in Fig. 3B. The significantly improved performance on D7 shows that the repeated PBM treatments are likely more effective than a single treatment (Salehpour et al., 2017; Yang et al., 2018). Nonetheless, future studies are needed for determining the exact therapy regimen to achieve optimal effectiveness of the PBM treatment.

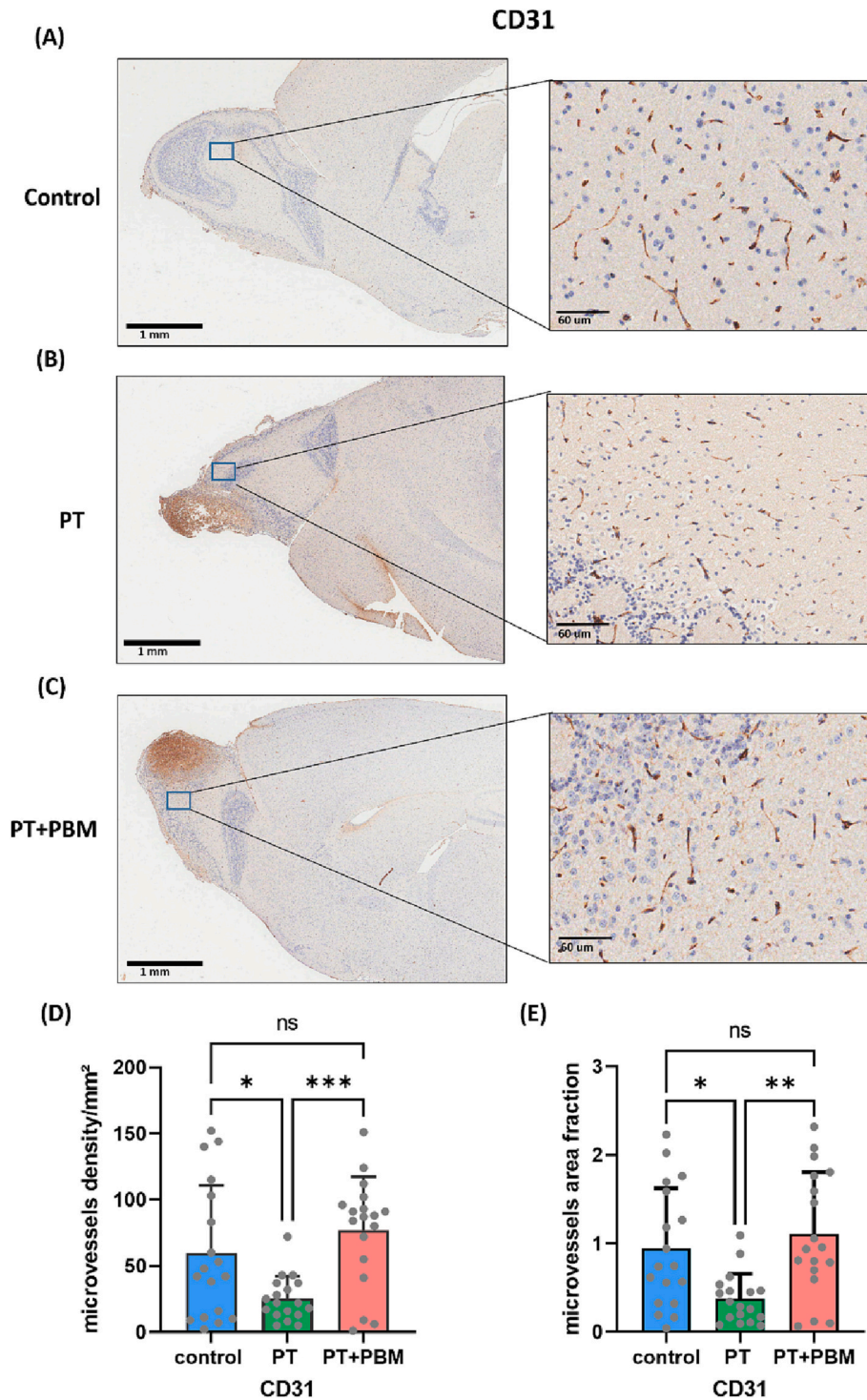


Fig. 7. PBM enhances the expression of CD31 after PT. (A-C) expression of CD31 in control, PT, PT + PBM with high magnification image. (D) Quantification of CD31count for control, PT, and PT + PBM. (E) Quantification of the CD31 area. Samples were collected on day 8. Data are mean ± SD. (n = 6 animal per group, 3 areas per animal; *P < 0.05, **P < 0.01, ***P < 0.001; ns-not significant).

Interestingly, the changes in the latency time, indicated that the rate of function shifts at early stages predicted the recovery rate at the late stages. As shown in Fig. 4, we found out that the significant correlations, independent of the PBM treatments were present between the functional changes quantified over the D-1 ~ D3 and D3 ~ D7 periods. More remarkable, the correlation slopes were similar between the PT and PT + PBM groups. Such similarity indicates a possibility of the recovery mechanism shared by both the PT and PT + PBM groups, in which the

PBM treatments appeared to accelerate the recovery process while maintaining the nature of the recovery process.

During the pathological progression of ischemic stroke, management of the acute inflammatory response plays an essential role in the prognosis of patient outcomes. Although neuroinflammation, in general provides a defense mechanism that removes cell debris and promotes tissue repair at the initial stage of stroke progression, the prolonged presence of inflammatory factors could exert an adverse effect on the

functional recovery (Wyss-Coray and Mucke, 2002). Therefore, we posited that the attenuation of the pro-inflammatory cytokines is likely associated with protective mechanisms in the post-ischemic brain tissue (Sieber et al., 2011). As demonstrated in Fig. 5, PBM not only down-regulated the inflammatory cytokines after PT but also upregulated the levels of anti-inflammatory cytokines. Such dynamic levels of cytokines could play a vital role in the pathogenesis of stroke, which reciprocally poses as potential targets of therapeutic intervention (Jayaraj et al., 2019). Although the mechanisms are not yet well defined, we showed that the elevated expression of pro-inflammatory cytokines such as IL-1 α , IL-1 β , IL-16 after PT was significantly reduced by PBM. Also important, the levels of anti-inflammatory cytokines including IL-1ra, IL-4 and IL-10 were effectively elevated in the PT animals treated with PBM compared with the PT group (Yang et al., 2018). In this regard, our study showed that PBM reduces further deterioration of the olfactory function by inhibiting the inflammatory process as well as by enhancing the healing process by increasing the blood flow leading to tissue oxygenation and enhancing neurogenesis after stroke.

In addition, the upregulated CD31 demonstrated that PBM enhances the restorative blood vessel density in the olfactory bulb after PT, likely promoting the circulation-related recovery process (Buscemi et al., 2019). On the other hand, the reactive astrocytes (delineated by GFAP: see Fig. 6), which were significantly reduced in the PT + PBM group, can be functionally divided into both neuroinflammatory and neuro-protective types (A1 and A2) (Li et al., 2022). In contrary to the PBM-induced restoration of olfactory function, the neuroinflammatory type (A1) is known to possess a significant neurotoxicity after stroke and is associated with the worsening neurological prognosis (Guttenplan et al., 2021). We hypothesize that PBM selectively inhibits the activation of toxic astrocytes, for which future studies are warranted.

We also demonstrated that the elevated inflammatory mediators such as C5a, IL-1 α , IL-1 β , IL-16, IL17 and TNF- α which are known to promote neuronal apoptosis, aggravate brain injury, inhibit neurogenesis, promote adhesion molecules, and reduce the blood-brain barrier integrity (Barone et al., 1997; Ferrarese et al., 1999; Zhu et al., 2022) were significantly downregulated by PBM. Moreover, PBM highly enhanced the anti-inflammatory mediators like GM-CSF, IL-1ra, IL-4, and IL-10, previously reported to have neuroprotective effects by reducing inflammatory markers associated with risks of poor outcomes, thus promoting the stroke recovery (Theoret et al., 2016; Yang et al., 2018). On the contrary, also highly affected by PBM was the elevated level of sICAM-1 which is known to correlate with cerebral microbleeds and hemorrhagic transformation in stroke patients (Wu, Wu et al., 2018) participating in the deterioration of the post-stroke vascular function. For resolving such discrepancy, focused future studies are required to address the role of sICAM-1 in the post-stroke functional recovery and to reveal the mechanism of PBM in its expression.

To date, most animal stroke studies have focused on the cortical and hippocampal regions of the brain, which are associated with multiple dysfunctions encompassing learning, memory, motor, etc. Although the importance of the olfactory function and its implication in many neurodegenerative diseases has been reported frequently, there are only few lesion studies conducted directly on the olfactory bulb. In our rodent study, a novel window model exposing the olfactory bulb allowed an easy access for the optical in vivo modulation, while the effect of damage could be quantified by the olfactory function assessment test (e.g., BFT). From the translational perspective, future studies can be designed to optimize a transcranial PBM strategy for the post-stroke patients with a loss of olfactory function by employing transcranial near-infrared light helmets. Meanwhile, PBM can be also administered through the nasal cavity and stimulate the recovery process (Salehpour et al., 2020), thus making it a potential therapeutic option for COVID-19 patients who are prone to have olfactory dysfunction with the local tissue damage (Soares et al., 2021; de Souza et al., 2022; Marashian et al., 2022).

Although a few inflammatory factors were investigated in the current study, specific mechanisms underlying the functional recovery after

PBM are yet to be determined. Moreover, despite the significance of long-term recovery, the current study did not examine either extended therapy or permanent recovery. Further research is needed to investigate the lasting impact of various PBM treatment durations during the acute phase, as well as before and after reaching the chronic stage. Additional limitations of this study include the absence of infarct volume quantification and analysis of transcriptional changes associated with PBM therapy.

Nonetheless, based on the current findings, we concluded that the selective expressions of genes that have key roles in the stroke recovery process are promoted by PBM rather than the restoration of the infarcted tissue. The importance of our study lies in the demonstration of accelerated functional recovery by the PBM therapy. Moreover, such functional restoration can be emphasized for conducting feasibility investigations of PBM as a clinical therapy option to treat patients with various olfactory functional deficits.

5. Conclusion

Using photothrombosis (PT) in the olfactory bulb of mouse brain, we developed a new ischemic stroke model that is optically accessible and evaluated the efficacy of photobiomodulation (PBM) for treating the impaired olfaction behavior. Specifically, we showed that the daily PBM therapy could significantly improve the compromised olfactory function while exerting little effects on the normal healthy brains. These outcomes were additionally supported by the histopathological staining and cytokines assay, revealing the role of PBM for suppressing post-stroke inflammatory reactions. As a result, we PBM could be a promising therapy option at the acute stage of brain ischemia to accelerate the functional recovery process and possibly, for treating olfactory dysfunctions resulting from various etiological causes including COVID-19.

Disclosures

The authors declare no conflicts of interest

Declaration of Competing Interest

None.

Data availability

Data will be made available on request.

Acknowledgments

The authors thank Eun Jung Ahn for assisting in the Cytokine assay, Minsung Kim for helpful discussion, Akm Ashiquzzaman for assisting in CD31 analysis and Christine H. Hwang for reviewing the manuscript.

Funding: The work was supported by the GIST Research Institute (GRI) research collaboration grant funded by GIST in 2023, the AI-based GIST Research Scientist Project grant funded by the GIST in 2023, and the 2023 Joint Research Project of Institutes of Science and Technology, a grant from the National Research Foundation of Korea (N.R.F.) funded by the Korean government (MEST) (NRF-2019R1A2C2086003), and the Korea Medical Device Development Fund grant funded by the Korea government, the Ministry of Science and ICT, the Ministry of Trade, Industry and Energy, the Ministry of Health & Welfare, the Ministry of Food and Drug Safety (Project Number: 1711138096, KMDF_PR_220200901_0076), and the Brain Pool program funded by the Ministry of Science and ICT through the NRF of Korea (2022H1D3A2A01096513) for EC. This work was also supported by the Chonnam National University Hospital Biomedical Research Institute (BCRI22062: KHL).

Appendix A. Supplementary data

Supplementary data to this article can be found online at <https://doi.org/10.1016/j.expneurol.2023.114462>.

References

- Aimbire, F., Albertini, R., Pacheco, M.T., Castro-Faria-Neto, H.C., Leonardo, P.S., Iversen, V.V., Lopes-Martins, R.A., Bjordal, J.M., 2006. Low-level laser therapy induces dose-dependent reduction of TNF α levels in acute inflammation. *Photomed. Laser Surg.* 24 (1), 33–37.
- Alberts, J.R., Galef Jr., B.G., 1971. Acute anosmia in the rat: a behavioral test of a peripherally-induced olfactory deficit. *Physiol. Behav.* 6 (5), 619–621.
- Barone, F.C., Arvin, B., White, R.F., Miller, A., Webb, C.L., Willette, R.N., Lysko, P.G., Feuerstein, G.Z., 1997. Tumor necrosis factor- α . A mediator of focal ischemic brain injury. *Stroke* 28 (6), 1233–1244.
- Berman, M.H., Halper, J.P., Nichols, T.W., Jarrett, H., Lundy, A., Huang, J.H., 2017. Photobiomodulation with near infrared light helmet in a pilot, placebo controlled clinical trial in dementia patients testing memory and cognition. *J. Neurol. Neurosci.* 8 (1).
- Blesa, J., Przedborski, S., 2014. Parkinson's disease: animal models and dopaminergic cell vulnerability. *Front. Neuroanat.* 8, 155.
- Brann, J.H., Firestein, S.J., 2014. A lifetime of neurogenesis in the olfactory system. *Front. Neurosci.* 8, 182.
- Buscemi, L., Price, M., Bezzi, P., Hirt, L., 2019. Spatio-temporal overview of neuroinflammation in an experimental mouse stroke model. *Sci. Rep.* 9 (1), 507.
- Carnemolla, S.E., Hsieh, J.W., Sipione, R., Landis, B.N., Kumfor, F., Piguet, O., Manuel, A.L., 2020. Olfactory dysfunction in frontotemporal dementia and psychiatric disorders: a systematic review. *Neurosci. Biobehav. Rev.* 118, 588–611.
- Chao, L.L., Barlow, C., Karimpoor, M., Lim, L., 2020. Changes in brain function and structure after self-administered home photobiomodulation treatment in a concussion case. *Front. Neurol.* 11, 952.
- de Souza, V.B., Ferreira, L.T., Sene-Fiores, M., Garcia, V., Rodrigues, T.Z., de Aquino Junior, A.E., Bagnato, V.S., Panhoca, V.H., 2022. Photobiomodulation therapy for treatment olfactory and taste dysfunction COVID-19-related: a case report. *J. Biophotonics* 15 (8), e202200058.
- Dintica, C.S., Marseglia, A., Rizzuto, D., Wang, R., Seubert, J., Arfanakis, K., Bennett, D.A., Xu, W.L., 2019. Impaired olfaction is associated with cognitive decline and neurodegeneration in the brain. *Neurology* 92 (7), e700–e709.
- Doty, R.L., 2012. Olfactory dysfunction in Parkinson disease. *Nat. Rev. Neurol.* 8 (6), 329–339.
- Eissa, M., Salih, W.H.M., 2017. The influence of low-intensity He-Ne laser on the wound healing in diabetic rats. *Lasers Med. Sci.* 32 (6), 1261–1267.
- Ferrarese, C., Masciarucci, P., Zoia, C., Cavarretta, R., Frigo, M., Begni, B., Sarinella, F., Fratola, L., De Simoni, M.G., 1999. Increased cytokine release from peripheral blood cells after acute stroke. *J. Cereb. Blood Flow Metab.* 19 (9), 1004–1009.
- Ferraresi, C., Kaippert, B., Avci, P., Huang, Y.Y., de Sousa, M.V., Bagnato, V.S., Parizotto, N.A., Hamblin, M.R., 2015. Low-level laser (light) therapy increases mitochondrial membrane potential and ATP synthesis in C2C12 myotubes with a peak response at 3–6 h. *Photochem. Photobiol.* 91 (2), 411–416.
- Graziadei, P.P., Graziadei, G.A., 1979. Neurogenesis and neuron regeneration in the olfactory system of mammals. I. Morphological aspects of differentiation and structural organization of the olfactory sensory neurons. *J. Neurocytol.*
- Guttenplan, K.A., Weigel, M.K., Prakash, P., Wijewardhane, P.R., Hasel, P., Rufen-Blanchette, U., Munch, A.E., Blum, J.A., Fine, J., Neal, M.C., Bruce, K.D., Gitler, A.D., Chopra, G., Liddelow, S.A., Barres, B.A., 2021. Neurotoxic reactive astrocytes induce cell death via saturated lipids. *Nature* 599 (7883), 102–107.
- Hamblin, M.R., 2016. Shining light on the head: Photobiomodulation for brain disorders. *BBA Clin.* 6, 113–124.
- Hamblin, M.R., 2017. Mechanisms and applications of the anti-inflammatory effects of photobiomodulation. *AIMS Biophys.* 4 (3), 337–361.
- Hamblin, M.R., 2019. Photobiomodulation for Alzheimer's disease: has the light dawned? *Photonics* 6 (3).
- Hopkins, J.T., McLoda, T.A., Seegmiller, J.G., David Baxter, G., 2004. Low-level laser therapy facilitates superficial wound healing in humans: a triple-blind, sham-controlled study. *J. Athl. Train.* 39 (3), 223–229.
- Jayaraj, R.L., Azimullah, S., Beiram, R., Jalal, F.Y., Rosenberg, G.A., 2019. Neuroinflammation: friend and foe for ischemic stroke. *J. Neuroinflammation* 16 (1), 142.
- Kim, H., Kim, M.J., Kwon, Y.W., Jeon, S., Lee, S.Y., Kim, C.S., Choi, B.T., Shin, Y.I., Hong, S.W., Shin, H.K., 2022. Benefits of a skull-interfaced flexible and implantable multilight emitting diode Array for Photobiomodulation in ischemic stroke. *Adv. Sci. (Weinh.)* 9 (11), e2104629.
- Labat-gest, V., Tomasi, S., 2013. Photothrombotic ischemia: a minimally invasive and reproducible photochemical cortical lesion model for mouse stroke studies. *J. Vis. Exp.* 76.
- LaFerla, F.M., Green, K.N., 2012. Animal models of Alzheimer disease. *Cold Spring Harb. Perspect. Med.* 2 (11).
- Lapchak, P.A., 2010. Taking a light approach to treating acute ischemic stroke patients: transcranial near-infrared laser therapy translational science. *Ann. Med.* 42 (8), 576–586.
- Lapchak, P.A., Salgado, K.F., Chao, C.H., Zivin, J.A., 2007. Transcranial near-infrared light therapy improves motor function following embolic strokes in rabbits: an extended therapeutic window study using continuous and pulse frequency delivery modes. *Neuroscience* 148 (4), 907–914.
- Li, L., Zhou, J., Han, L., Wu, X., Shi, Y., Cui, W., Zhang, S., Hu, Q., Wang, J., Bai, H., Liu, H., Guo, W., Feng, D., Qu, Y., 2022. The specific role of reactive astrocytes in stroke. *Front. Cell. Neurosci.* 16, 850866.
- Marashian, S.M., Hashemian, M., Pourabdollah, M., Nasser, M., Mahmoudian, S., Reinhart, F., Eslaminejad, A., 2022. Photobiomodulation improves serum cytokine response in mild to moderate COVID-19: the first randomized, double-blind, placebo controlled, pilot study. *Front. Immunol.* 13, 929837.
- Naeser, M.A., Saltmarche, A., Krengel, M.H., Hamblin, M.R., Knight, J.A., 2011. Improved cognitive function after transcranial, light-emitting diode treatments in chronic, traumatic brain injury: two case reports. *Photomed. Laser Surg.* 29 (5), 351–358.
- Oron, A., Oron, U., Streeter, J., De Taboada, L., Alexandrovich, A., Trembovler, V., Shohami, E., 2012. Near infrared transcranial laser therapy applied at various modes to mice following traumatic brain injury significantly reduces long-term neurological deficits. *J. Neurotrauma* 29 (2), 401–407.
- Rebholz, H., Braun, R.J., Ladage, D., Knoll, W., Kleber, C., Hassel, A.W., 2020. Loss of olfactory function-early indicator for Covid-19, other viral infections and neurodegenerative disorders. *Front. Neurol.* 11, 569333.
- Salehpour, F., Hamblin, M.R., 2020. Photobiomodulation for Parkinson's disease in animal models: a systematic review. *Biomolecules* 10 (4).
- Salehpour, F., Ahmadian, N., Rasta, S.H., Farhoudi, M., Karimi, P., Sadigh-Eteghad, S., 2017. Transcranial low-level laser therapy improves brain mitochondrial function and cognitive impairment in D-galactose-induced aging mice. *Neurobiol. Aging* 58, 140–150.
- Salehpour, F., Gholipour-Khalili, S., Farajdokht, F., Kamari, F., Walski, T., Hamblin, M.R., DiDuro, J.O., Cassano, P., 2020. Therapeutic potential of intranasal photobiomodulation therapy for neurological and neuropsychiatric disorders: a narrative review. *Rev. Neurosci.* 31 (3), 269–286.
- Sieber, M.W., Claus, R.A., Witte, O.W., Frahm, C., 2011. Attenuated inflammatory response in aged mice brains following stroke. *PLoS One* 6 (10), e26288.
- Soares, L.E.S., Guirado, M.M.G., Berlingieri, G., Ramires, M., Lyra, L., Teixeira, I.S., Oliveira, P.C., Tateno, R.Y., Palma, L.F., Campos, L., 2021. Intranasal photobiomodulation therapy for COVID-19-related olfactory dysfunction: a Brazilian multicenter case series. *Photodiagn. Photodyn. Ther.* 36, 102574.
- Theoret, J.K., Jadavji, N.M., Zhang, M., Smith, P.D., 2016. Granulocyte macrophage colony-stimulating factor treatment results in recovery of motor function after white matter damage in mice. *Eur. J. Neurosci.* 43 (1), 17–24.
- Thunshelle, C., Hamblin, M.R., 2016. Transcranial low-level laser (light) therapy for brain injury. *Photomed. Laser Surg.* 34 (12), 587–598.
- Wehling, E., Naess, H., Wollschlaeger, D., Hofstad, H., Bramerson, A., Bende, M., Nordin, S., 2015. Olfactory dysfunction in chronic stroke patients. *BMC Neurol.* 15, 199.
- Wesson, D.W., Levy, E., Nixon, R.A., Wilson, D.A., 2010. Olfactory dysfunction correlates with amyloid-beta burden in an Alzheimer's disease mouse model. *J. Neurosci.* 30 (2), 505–514.
- Wu, B.N., Wu, J., Hao, D.L., Mao, L.L., Zhang, J., Huang, T.T., 2018. High serum sICAM-1 is correlated with cerebral microbleeds and hemorrhagic transformation in ischemic stroke patients. *Br. J. Neurosurg.* 32 (6), 631–636.
- Wyss-Coray, T., Mucke, L., 2002. Inflammation in neurodegenerative disease – a double-edged sword. *Neuron* 35 (3), 419–432.
- Xuan, W., Agrawal, T., Huang, L., Gupta, G.K., Hamblin, M.R., 2015. Low-level laser therapy for traumatic brain injury in mice increases brain derived neurotrophic factor (BDNF) and synaptogenesis. *J. Biophotonics* 8 (6), 502–511.
- Yang, M., Crawley, J.N., 2009. Simple behavioral assessment of mouse olfaction. *Curr. Protoc. Neurosci.* 8, 24.
- Yang, L., Tucker, D., Dong, Y., Wu, C., Lu, Y., Li, Y., Zhang, J., Liu, T.C., Zhang, Q., 2018. Photobiomodulation therapy promotes neurogenesis by improving post-stroke local microenvironment and stimulating neuroprogenitor cells. *Exp. Neurol.* 299 (Pt A), 86–96.
- Yeh, C.F., Chuang, T.Y., Lan, M.Y., Chin, Y.C., Wang, W.H., Lin, Y.Y., 2019. Excessive expression of microglia/macrophage and proinflammatory mediators in olfactory bulb and olfactory dysfunction after stroke. *In Vivo* 33 (6), 1893–1899.
- Zhu, H., Hu, S., Li, Y., Sun, Y., Xiong, X., Hu, X., Chen, J., Qiu, S., 2022. Interleukins and ischemic stroke. *Front. Immunol.* 13, 828447.